Chapter 9
Applications of Calorimetry on Polymer Nanocomposites

Qingliang He, Xingru Yan, Jiang Guo, Xi Zhang, Huige Wei, Dawei Jiang, Xin Wei, Daowei Ding, Suying Wei, Evan K. Wujcik, and John Zhanhu Guo

9.1 Introduction

The objective of calorimetry is to measure the heat in specific ways. Microscale combustion calorimetry (MCC) is also named as pyrolysis–combustion flow calorimetry [1], which has the dynamic capability to measure maximum rate of heat release and other heat-related parameters using milligram-sized samples. MCC achieves this objective by (1) rapidly heating sample to a controlled pyrolysis state under an inert condition (nitrogen) or a mixture of oxygen and nitrogen followed by (2) rapid high-temperature oxidization (combustion) of the pyrolyzate in excess oxygen, which simulates the combustion [2]. Thus, MCC reproduces both the solid phase state (pyrolysis) and the gas phase state (combustion) chemical processes of flaming combustion of polymeric materials and determines the heat release rate

Q. He • X. Yan • J. Guo • J.Z. Guo (✉)
Integrated Composites Laboratory (ICL), Department of Chemical and Biomolecular
Engineering, University of Tennessee, Knoxville, TN 37996, USA
e-mail: zguo10@utk.edu

X. Zhang • H. Wei • D. Jiang
Department of Chemistry and Biochemistry, Lamar University, Beaumont, TX 77710, USA

X. Wei • D. Ding • E.K. Wujcik
Dan F. Smith Department of Chemical Engineering, Lamar University,
Beaumont, TX 77710, USA

S. Wei
Department of Chemistry and Biochemistry, Lamar University, Beaumont, TX 77710, USA

Dan F. Smith Department of Chemical Engineering, Lamar University,
Beaumont, TX 77710, USA

J.Z. Guo (✉)
Chemical and Biomolecular Engineering Department, University of Tennessee,
Knoxville, TN 37996, USA

based on the oxygen consumption in a "non-flaming" oxidation process. Parameters including heat release capacity (HRC), specific heat release rate (HRR) at different temperatures, peak heat release rate (PHRR), temperature at PHRR (T_{PHRR}), and total heat release (THR) can be obtained from MCC. Meanwhile, full width half height (FWHH) and final residual percentage can be calculated [3].

The heat-related parameters collected from MCC, especially the rate of heat release, are the most important and the single key to evaluate the fire hazards of one material. According to its standard testing method ASTM D-7309, the specific HRR at time t can be calculated by Eq. (9.1):

$$\text{HRR}_{(t)} = \frac{EOF}{m_o} \Delta \left[O_2 \right]_{(t)}$$ (9.1)

The first term E refers to the heat released by complete combustion of a sample per unit mass of O_2 consumed, which is an empirical constant (~13.1 kJ/g-O_2). The second term (ρ) is the density of O_2 at ambient condition. The third term F is the volumetric flow rate of the combustion stream at ambient temperature and pressure measured at the terminal flow meter. The forth term $\Delta[O2](t)$ is the change in the concentration (volume fraction) of O_2 in the gas stream due to combustion measured at the oxygen sensor at time t. The last term m_0 is the original mass of one testing sample. It is obvious that the oxygen consumption ($\Delta[O2](t)$) is the key factor to determine the value of HRR.

HRC is another important parameter to determine the flammability of one material. HRC is calculated using Eq. (9.2):

$$\text{HRC} = \frac{PHRR}{\beta}$$ (9.2)

PHRR is the maximum specific heat release rate during a controlled thermal decomposition, and β is the average heating rate.

For exploration of multifunctional polymer nanocomposites, especially for the investigation on these flame-retardant-treated polymer nanocomposites, it is useful and necessary to determine the fire risks/hazards based on these combustion parameters. In addition, these parameters are also important guidance for the industrial applications.

Differential scanning calorimetry (DSC) is one of the most widely used calorimetry for determining the endothermic and exothermic heat during the melting and cooling process for one material via measuring the change of the difference in the heat flow rate to one testing sample and to a standard reference sample while they are subjected to a controlled temperature program [4]. In one typical non-isotherm DSC heat-cool-heat cycle, the melting and cooling thermograms including maximum endothermic melting temperature (T_m), the maximum exothermic crystalline

temperature (T_c), the enthalpy of fusion (ΔH_m), and the enthalpy of crystallization (ΔH_c) can be obtained [5]. Meanwhile, the crystallization fraction (F_c) of one semicrystalline polymer or its nanocomposites can also be calculated according to Eq. (9.3):

$$F_c = \Delta H_m / \left[\Delta H_m{}^\circ \cdot \left(1-x\right) \right] \qquad (9.3)$$

where ΔH_m is the measured enthalpy of fusion (integration of the melting peak area under the baseline of DSC curves); $\Delta H_m{}^\circ$ is the enthalpy of fusion of 100 % crystalline polymer (here, e.g., the theoretical value of $\Delta H_m{}^\circ$ for 100 % crystalline polypropylene is 209 J/g [6]; and the theoretical value of $\Delta H_m{}^\circ$ for 100 % crystalline polyethylene is 293 J/g) [5a, 7]. The x is the loading of the fillers in the polymer matrix. If pure polymer is used, the x here equals to zero.

In order to prove the improvement after fabricating one polymer into its polymer matrix nanocomposites, it is of great importance to determine the differences of their physicochemical properties. The calorimetry including both the DSC and MCC is powerful to obtain heat-related parameters, which are useful to evaluate the performance of the obtained polymer matrix nanocomposites in terms of improved melting and crystalline behaviors and reduced flammability and lower fire risks for certain applications.

The synthesis procedures of the HDPE and PP nanocomposites were reported elsewhere [3, 5, 8]. The non-isotherm DSC melting and cooling thermograms of pristine polyolefins and their polymer matrix nanocomposites were carried out by using DSC on a TA Instruments Q-2000 calorimeter. Approximately 5–10 mg sample was encapsulated in a standard aluminum pan and heated from 0 to 250 °C at a heating rate of 10 °C/min under a nitrogen flow rate of 50 mL/min. Prior to cooling down to room temperature, the sample was set to stay isotherm at 200 °C for 3 min. After that, the samples were reheated again from room temperature to 200 °C. The data enclosed were collected from the first cooling and the second heating procedures in order to remove the heat history.

The heat release-related parameters were collected by using a microscale combustion calorimetry (MCC, type 2, Govmark, Inc.) with milligram-sized samples according to the standard testing method ASTM D7309-2007 (Method A). These parameters were recorded and utilized to evaluate the fire hazards [2, 3]. To be specific, the heat release-related parameters including specific heat release rate (HRR) at different temperatures, peak heat release rate (PHRR), temperature at PHRR (T_{PHRR}), and total heat release (THR) were obtained from MCC. Meanwhile, full width half height (FWHH) and final residual percentage were calculated. In a typical measurement, about 3–5 mg sample was heated from 90 to 600 °C under a heating rate of 1 °C/s in a continuous stream of nitrogen flowing at 80 mL/min. The thermal decomposition products (also called as "fuel gases") were mixed with a 20 mL/min stream of oxygen before entering a 900 °C combustion furnace to complete the non-flaming combustion.

9.2 Discussion

The crystallization behaviors of semicrystalline hydrocarbon polymers like poly-
ethylene and polypropylene have been widely studied. Due to their intrinsic semi-
crystallinity, the crystallization behaviors can be strongly affected by the nanofillers
which have been introduced into these polymer matrices. For example, the DSC
melting and crystallization plots of the pristine high-density polyethylene (namely,
as HDPE) and its polymer matrix nanocomposites filled with in situ-formed iron@
iron oxide (Fe@Fe$_2$O$_3$) nanoparticles (NPs) were demonstrated in Fig. 9.1a, b. The
detailed data including melting peak temperature, T_m; crystallization peak tempera-
ture, T_c; enthalpy of fusion, ΔH_m; enthalpy of crystallization, ΔH_c; and crystalliza-
tion fraction, F_c were summarized in Table 9.1. For 100 % crystalline polyethylene,
the best experimental heat of fusion is 4.1 kJ/mol of CH$_2$, which approximately
equals to 293 J/g [7]. The pristine HDPE demonstrates a T_m at 129.8 °C and a T_c at
116.7 °C. The F_c is 62.0 % as calculated from Eq. 9.3. Compared with pristine
HDPE, the melting and crystalline peak temperatures of all the nanocomposites
with different filler loadings stayed almost unchanged as shown in Fig. 9.1.

These phenomena indicate that the original crystal structure of the hosting HDPE
matrix remains unchanged in spite of the incorporation of the in situ-synthesized
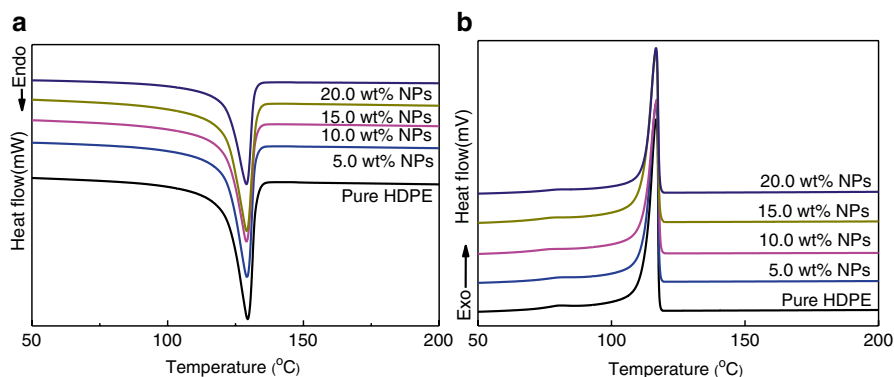
Fig. 9.1 DSC curves of pure HDPE and its nanocomposites: (**a**) second heating and (**b**) first cool-
ing cycle [5a] (Reproduced from Ref. [5a] with permission from the Elsevier)

Table 9.1 DSC characteristics of the HDPE and its nanocomposites [5a]

Composition	T_m (°C)	ΔH_m (J/g)	T_c (°C)	ΔH_c (J/g)	F_c (%)
Pure HDPE	129.8	181.8	116.7	169.3	62.0
5.0 wt% NPs	129.3	167.9	116.7	151.5	60.3
10.0 wt% NPs	129.3	157.2	116.7	139.1	59.6
15.0 wt% NPs	129.3	151.5	116.7	147.0	60.8
20.0 wt% NPs	129.3	140.9	116.7	126.7	60.1

Reproduced from Ref. [5a] with permission from the Elsevier

Fig. 9.2 DSC curves of pure PP and its nanocomposites with different loadings of Co@Co$_3$O$_4$ NPs [5b] (Reprinted with permission from Ref. [5b]. Copyright (2013) American Chemical Society)
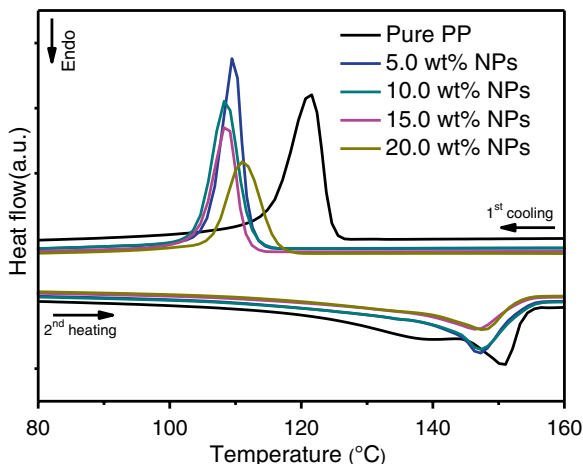
NPs. However, the F_c (Table 9.1) decreased slightly (3–4 %) after the NPs were introduced into the hosting polymer matrix. The ΔH_m of HDPE decreased significantly from 181.8 to 167.9 J/g when 5.0 wt% NPs were incorporated in the HDPE matrix and further decreased to 140.9 J/g in the PNCs with 20.0 wt% particle loading. Since the crystalline structure of HDPE didn't change in all the nanocomposite samples after adding the Fe@Fe$_2$O$_3$ NPs as evidenced from X-ray diffraction pattern [5a], the decrease of the enthalpy of fusion was probably caused by the decrease in the crystalline size of HDPE molecules [9].

Upon heating in xylene, the hydrocarbon HDPE chains were relaxed and the NPs were formed among the relaxed chains. The lower F_c of these nanocomposites is attributed to the fact that the NPs are able to disturb the continuity of the HDPE chains and thus introduce more grain boundaries and defects in hosting matrix; and the F_c is suppressed accordingly.

Similar situation was also observed in the polypropylene (PP) magnetic polymer matrix nanocomposites reinforced with in situ-formed cobalt@cobalt oxide (Co@Co$_3$O$_4$) NPs in the presence of surfactant maleic anhydride grafted polypropylene (MAPP) [5b]. Compared with the PP matrix, all these polymer matrix nanocomposites show a slightly decreased T$_m$ and a significantly decreased T$_c$ (Fig. 9.2). Meanwhile, significant decreases in ΔH_m and ΔH_c are observed. ΔH_m decreases significantly from 87.0 to 80.8 J/g when 5.0 wt% NPs were introduced into PP matrix. The ΔH_m and ΔH_c were observed to further decrease to 60.1 and 61.7 J/g, respectively, when the particle loading was further increased to 20.0 wt%. The F_c is observed to decrease after the incorporation of the NPs (F_c decreased from 41.6 to 40.7 % when polymer matrix was incorporated with 5.0 wt% NPs, then decreased to 35.9 %, when particle loading was further increased to 20.0 wt% NPs) [5b]. This suggests that the crystallization of PP was partially suppressed, as the Co@Co$_3$O$_4$ NPs could act as defects and thus introduced more grain boundaries, which effectively hindered the crystallization of PP segments [10].

Fig. 9.3 DSC curves of PP/1 % CNTs, nanocomposites of PP/1 % f-CNTs, nanocomposites of PP/1.0 % CNTs/1 % MAPP (1 or 2), and PP/1.0 % f-CNTs/1 % MAPP (1 or 2) [8]. MAPP-1: (molecular weight $M_n = 800$), MAPP-2 ($M_n = 8000$) (Reproduced from Ref. [8] with permission from the John Wiley and Sons)
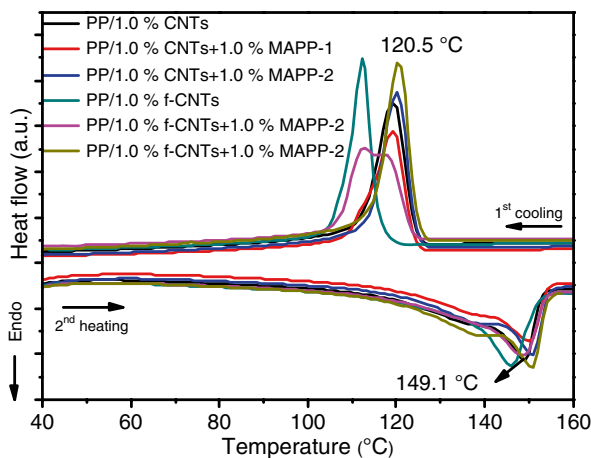
Another example of the melting and crystallization behaviors of PP polymer matrix nanocomposites filled with untreated and treated carbon nanotubes (with/without the aid of surfactant MAPP) was illustrated in Fig. 9.3 [8]. It can be seen that pure PP has a T_m at 150.7 °C and a ΔH_m of 101.8 J/g with F_c of 48.7 %. When 1.0 wt% untreated carbon nanotubes (CNTs) were added in the PP matrix, the T_m was slightly decreased (149.1 °C); however, ΔH_m was significantly decreased from 101.8 to 83.3 J/g, leading to a decreased F_c of 40.3 %. When adding 1.0 wt% MAPP (type 1 or 2), T_m stayed almost unchanged compared with that of pure PP; however, ΔH_m was further decreased to 74.4 J/g for adding 1.0 wt% MAPP-1 and increased to 88.2 J/g for adding 1.0 wt% MAPP-2, respectively. The corresponding calculated F_c was 36.3 and 42.6 %. For either the PP/1 % CNTs or PP/1 % CNTs/1 % MAPP (type 1 or 2), there was no obvious change of T_c, indicating that no strong restriction of PP crystallization was taken place.

The crystallization of PP main chains was significantly restricted when introducing 1.0 wt% surface-treated CNTs (namely, as f-CNTs) in the PP matrix: T_m decreased to 146.1 °C and T_c decreased to 112.5 °C, which represents 4.6 and 8.8 °C decrease, respectively, along with a decreased F_c of 37.3 %. In combination with 1.0 wt% f-CNTs and 1.0 wt% MAPP-1, all these parameters were slightly changed as shown in Table 9.2. However, when combining 1 % f-CNTs and 1 % MAPP-2, the ΔH_m was increased to 92.1 J/g, corresponding to an F_c of 44.5 %. Meanwhile, T_m (146.1 °C) and T_c (120.5 °C) are similar to those of pure PP.

Usually, for semicrystalline polymer like PP, the introduction of CNTs into the polymer matrix can lead to an earlier crystallization (increase T_c) compared to pure polymer due to the fact that the heterogeneous nucleating effect of CNTs can accelerate the crystallization when polymer is cooled upon melt [11]. However, the decrease of T_c observed here is probably attributed to the non-crystallizable barrier effect of the agglomerated f-CNTs in the PP matrix [11b]. Therefore, the fillers can act as non-crystallizable barriers to disturb the crystal growth of polymer crystallization, which inversely decelerates the crystallization. Furthermore, the fillers may also hinder the mobility of polymer chains, which in turn restricts the growth of the crystallites [12].

**Table 9.2** DSC data of pure PP and PP/CNT nanocomposites

Composition	T_m (°C)	ΔH_m (J/g)	T_c (°C)	ΔH_c (J/g)	F_c (%)
PP	150.7	101.8	121.3	104.7	48.7
PP/1 % CNTs	149.1	83.3	119.2	88.8	40.3
PP/1 % CNTs + 1 % MAPP-1	150.3	74.4	119.2	80.6	36.3
PP/1 % CNTs + 1 % MAPP-2	150.6	88.2	120.1	89.7	42.6
PP/1 % f-CNTs	146.1	77.2	112.5	83.4	37.3
PP/1 % f-CNTs + 1 % MAPP-1	148.5	77.7	112.5	85.4	38.0
PP/1 % f-CNTs + 1 % MAPP-2	150.7	92.1	120.5	98.1	44.5

Reproduced from Ref. [8] with permission from the John Wiley and Sons

In addition to the decreased T_c, the peak-broadening effects in the PP/1.0 % f-CNTs and PP/1.0 % f-CNTs/1.0 % MAPP-1 PNCs were also observed during the exothermic crystallization cycle, indicating the formation of imperfect polymer crystallites and the size distribution-broadening effect of thus formed crystallites [13]. The T_c (112.5 °C) of the PP/1.0 wt% f-CNTs/1.0 wt% MAPP-1 was further decreased compared with that (119.2 °C) of the PP/1.0 wt% CNTs, indicating a stronger barrier effect to the PP crystallization, while T_c was not significantly changed when MAPP-2 (120.5 °C) was introduced in the PP matrix since the larger free volume has been introduced (Fig. 9.3).

MCC was utilized to determine the heat release-related flammability parameters and further evaluate the fire hazards of pure PP, PP/20.0 wt% Co, and PP/20.0 % Co polymer matrix nanocomposites stabilized with two different molecular weight surfactants PP-g-MA [3]. PP-g-MA (S) ($M_n \approx 800$) is a gel-like propylene–hexene copolymer with one maleic anhydride (MA) group at one terminal and the other MA grafted on the main chain; and PP-g-MA (L) ($M_n \approx 2500$) is a solid homo-polypropylene with one terminal MA through Alder–ene reaction [14]. Figure 9.4 demonstrated the HRR vs. temperature curves, and Table 9.3 showed the detailed heat release parameters. HRR is the single most important parameter to assess the fire hazard of one flammable material [15]. Pure PP is a highly flammable material as the PHRR observed here of 1513.0 w/g. Adding 5 % PP-g-MA (L/S) slightly decreased the flammability as evidenced by the small amounts of reduction in HRC, PHRR, and THR (Table 9.3), which were apparently due to the less gas fuels generated from the oxygen-containing PP-g-MA (L/S) than pure hydrocarbon PP. In addition, the initial thermal decomposition and T_{PHRR} were similar to these of pure PP.

When adding 20.0 wt% Co NPs into PP matrix, PHRR was decreased from 1513.0 to 1024.0 W/g (~32.3 % reduction), THR was decreased from 40.6 to 27.7 W/g (~31.8 % reduction); and the initial decomposition temperature was enhanced upon adding the Co NPs (Fig. 9.4). Apparently, with excluding the dilution of combustible PP through the 20.0 wt% noncombustible Co loading, an additional 12.3 % decrease in HRR and 11.8 % decrease in THR indicated a flame retardancy effect of these in situ-synthesized Co NPs. Therefore, the HRR reduction
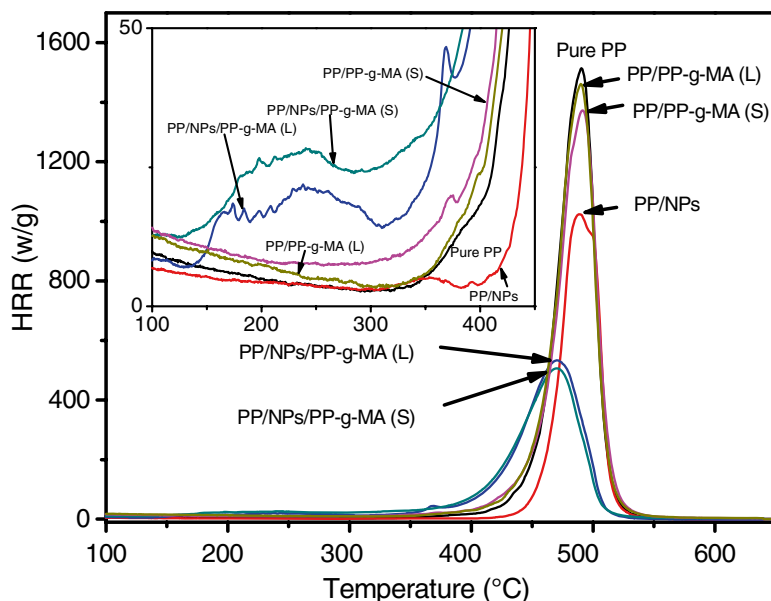
Fig. 9.4 Heat release rate curves of pure PP, PP/PP-g-MA, PP/20.0 % Co PNCs, and PP/20.0 % Co nanocomposites stabilized with two different molecular weight PP-g-MAs. Insert is enlarged initial low-temperature decomposition between 100 and 400 °C [3] (Reproduced from Ref. [3] with permission from the Royal Society of Chemistry)

Table 9.3 Heat release data of the PP and its nanocomposites with Co NPs [3]

Composition	HRC (J/g-k)	PHRR (W/g)	PHRR reduction (%)	T_{PHRR} (°C)	THR (KJ/g)	FWHH (s)
Pure PP	1187.0	1513.0	/	490.4	40.6	24.2
PP/PP-g-MA(L)	1150.0	1454.0	3.9	491.1	40.3	25.1
PP/PP-g-MA(S)	1077.0	1366.0	9.7	489.9	39.8	25.9
PP/20.0 % NPs	809.0	1024.0	32.3	489.9	27.7	23.7
PP/20.0 % NPs/ PP-g-MA(L)	417.0	532.4	64.8	471.0	25.6	39.7
PP/20.0 % NPs/ PP-g-MA(S)	395.0	500.8	66.9	471.0	25.1	41.0

Reproduced from Ref. [3] with permission from the Royal Society of Chemistry

here suggests a slower generation rate of combustible volatiles from the random chain scission of PP backbones in the presence of Co NPs, which can be considered as a barrier effect for the flame retardancy mechanism. During the decomposition, heat and mass transfers between gas and condense phases were slowed down by forming an insulating layer when these PNCs were exposed under heat, and thus fast decomposition of the polymeric PP matrix was suppressed [16].
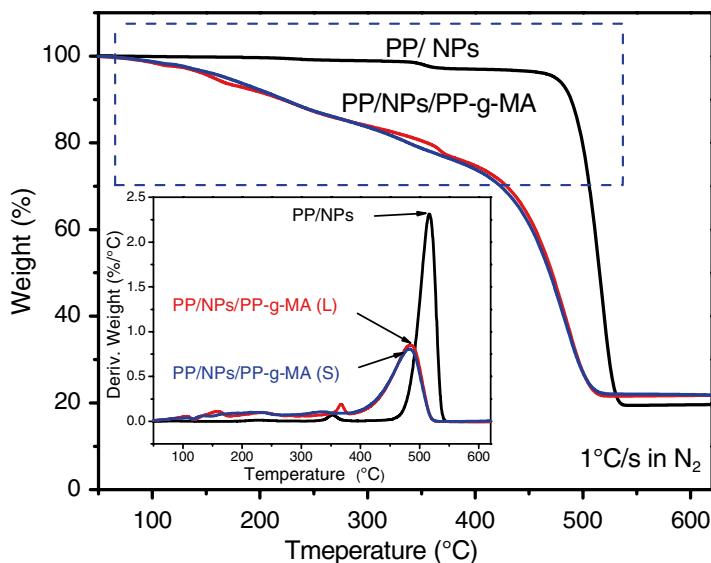
Fig. 9.5 TGA and DTA curves of PP/20.0 % Co MPNCs and PP/20.0 % Co PNCs stabilized with two PP-g-MAs under a heating rate of 1 °C/s (60 °C/min) [3] (Reproduced from Ref. [3] with permission from the Royal Society of Chemistry)

Synergistic effect in reducing flammability was observed when adding 5.0 % to both PP-g-MAs in the PP/20.0 wt% Co NP system (Fig. 9.4). HRC and PHRR were observed to decrease sharply, i.e., PHRR was further decreased from 1024.0 to 532.4 W/g in the case of PP/PP-g-MA (L)/Co PNCs or to 500.8 W/g in the case of PP/PP-g-MA (S)/Co PNCs when 5.0 % PP-g-MA was added in the PP/Co PNCs. Meanwhile, THR was further slightly decreased from 27.7 to 25.6 KJ/g with the addition of 5.0 % PP-g-MA (L) or to 25.1 KJ/g with the addition of 5.0 % PP-g-MA (S) into PP/20.0 % Co PNCs. Since PP-g-MA is only a polymeric additive serving as surfactant, this remarkable decrease in the flammability of PP by Co NPs and PP-g-MA has to be in its unique pathway. Although the conventional synergistic effect (such as nitrogen–phosphorus [17], phosphorus–silicon [18]) on flame-retardant polymer matrix nanocomposites has been extensively studied and reported, the synergistic effect between PP-MA and Co NPs has rarely been demonstrated. In addition, when either PP-g-MA was added in the PP/20.0 % Co system, a small amount of HRR was observed during the initial thermal decomposition stage (around 100–300 °C), and T_{PHRR} was decreased to 471.0 °C (shown in the insert of Fig. 9.4).

In order to further understand the synergism between PP-g-MA and Co NPs in dramatically reducing the flammability of PP matrix, a fast thermal degradation test was performed by thermogravimetric analysis (TGA) and differential thermal analysis (DTA) through using the identical heating condition as MCC measurements – a heating rate of 60 °C/min (1 °C/s) under nitrogen (TGA and DTA curves shown in Fig. 9.5). MCC measurements here were performed through using an inert sample thermal

degradation procedure to pyrolyze the sample into combustible gas volatiles followed by a non-flaming oxidation of these volatiles. The fast thermal degradation by TGA can illustrate the dynamic sample weight loss under temperature ramping at a constant high heating rate (1 °C/s); meanwhile, the derivative weight loss (%/°C) from the insert of Fig. 9.5 can reproduce the thermal degradation stage of MCC clearly. Therefore, the degradation and weight loss processes can be demonstrated simultaneously.

It is observed that the addition of 5.0 % PP-g-MA (L/S) barely decreased the initial thermal degradation temperature of PP, while 20.0 % Co NPs increased the initial thermal degradation of PP as evidenced by the higher thermal degradation temperature than that of pure PP (no detectable HRR increase before 400 °C, shown in the insert of Fig. 9.4). However, the degradation of PP/5.0 % PP-g-MA (L/S)/20.0 % Co NPs was definitely altered by the evidence of: broad HRR peaks appeared in the range of 130–310 °C (insert of Fig. 9.4) and ~18.0 % weight loss within the thermal degradation temperature of 100–310 °C from the TGA curves (Fig. 9.5). When exposed to heat flux at elevated temperature from 80 to 650 °C, the thermal degradation of PP under inert atmosphere was initiated primarily by chain scission and chain transfer; then reductions in molecular weight were first observed at 227 to 247 °C, and gas volatiles became significant above 302 °C. Finally, ignition of PP was observed at a surface temperature of 337 °C [19], consistent with the initial HRR jump at ~330 °C observed from MCC. Meanwhile, the addition of 5.0 % PP-g-MA (L/S) has limited influence on initiating the degradation of the PP matrix. With 20.0 % Co NPs, only shielding effect functioned as barrier for reducing the HRR through slowing and delaying the release of gas volatiles [16]. When adding PP-g-MA together with Co NPs in the PP matrix, the catalytic effect was responsible for lowering the initial thermal degradation temperature of the resulted PNCs (from 330 °C for pure PP to ~100–130 °C for the PNCs) and led to a smaller HRR in the range of 100–310 °C due to a small amount of gas volatiles released from bulk material. Probable mechanism includes the random chain scission of C–C bond of PP backbone to generate hydrocarbon radicals during initial decomposition, the formation of lower hydrocarbons such as propylene from further degradation of these hydrocarbon radicals, the β-scission and abstraction of H radicals from other hydrocarbons to produce a new hydrocarbon radicals during propagation stage, and finally the disproportionation or recombination of two radicals as termination reaction [20]. Meanwhile, slightly similar to the "smoldering" fire, a substantial fraction of the total mass of PP/5.0 % PP-g-MA (L/S)/Co PNCs (~18.0 %) was consumed during 100–310 °C subjected to a slow heat release process, effectively decreased the total available gas volatiles, which would generate large quantity of heat under higher temperatures. In addition, the strong interfacial adhesion between Co NPs and PP matrix through PP-g-MA was responsible for the sharply suppressed mass loss rate as observed reduction in PHRR (Figs. 9.4 and 9.5). Another important parameter, full width half height (FWHH), of the PP/PP-g-MA/Co PNCs was much wider than those of pure PP, PP/PP-g-MA, and PP/Co PNCs (Table 9.3) and further proved a longer combustion period upon introducing the PP-g-MA and Co NPs in the PP matrix. This is another sign of lower fire hazard of the PP/PP-g-MA/ Co PNCs.

9.3 Conclusion

To summarize, we have demonstrated the powerful capability of DSC and MCC to study the melting and crystallization behaviors and heat release-related flammability parameters. The melting and crystallization behaviors of both pristine polymers and their polymer matrix nanocomposites are of great importance to understand how and why the nanofillers changed the intrinsic properties of polymer backbones and can thus give further insight to predict and guide material design for optimal industrial applications. The heat release-related parameters including heat release rate and heat release capacity are paramount to determine the flammability of both the polymers and their nanocomposites. Along with other techniques such as thermogravimetric analysis, the change of thermal degradation pathways after introducing nanofillers into polymer matrix can be determined, and the flame retardancy mechanism can thus be understood by this powerful calorimetry.

References

1. (a) Lyon RE, Walters R, Stoliarov S (2007) Screening flame retardants for plastics using microscale combustion calorimetry. Polym Eng Sci 47(10):1501–1510; (b) Lyon RE, Walters RN (2004) Pyrolysis combustion flow calorimetry. J Anal Appl Pyrolysis 71(1):27–46; (c) Lyon R, Walters R, Stoliarov S (2007) Thermal analysis of flammability. J Therm Anal Calorim 89(2):441–448
2. Yang CQ, He Q, Lyon RE, Hu Y (2010) Investigation of the flammability of different textile fabrics using micro-scale combustion calorimetry. Polym Degrad Stab 95(2):108–115
3. He Q, Yuan T, Wei S, Guo Z (2013) Catalytic and synergistic effects on thermal stability and combustion behavior of polypropylene: influence of maleic anhydride grafted polypropylene stabilized cobalt nanoparticles. J Mater Chem A 1(42):13064–13075
4. Höhne G, Hemminger W, Flammersheim H-J (2003) Differential scanning calorimetry. Springer Science & Business Media, Berlin - Heidelberg
5. (a) He Q, Yuan T, Zhu J, Luo Z, Haldolaarachchige N, Sun L, Khasanov A, Li Y, Young DP, Wei S (2012) Magnetic high density polyethylene nanocomposites reinforced with in-situ synthesized Fe@ FeO core-shell nanoparticles. Polymer 53(16):3642–3652; (b) He Q, Yuan T, Zhang X, Luo Z, Haldolaarachchige N, Sun L, Young DP, Wei S, Guo Z (2013) Magnetically soft and hard polypropylene/cobalt nanocomposites: role of maleic anhydride grafted polypropylene. Macromolecules 46(6):2357–2368
6. (a) Carlson ED, Krejchi MT, Shah CD, Terakawa T, Waymouth RM, Fuller GG (1998) Rheological and thermal properties of elastomeric polypropylene. Macromolecules 31(16):5343–5351; (b) Rozanski A, Galeski A, Debowska M (2011) Initiation of cavitation of polypropylene during tensile drawing. Macromolecules 44:20–28
7. Wunderlich B, Czornyj G (1977) A study of equilibrium melting of polyethylene. Macromolecules 10(5):906–913
8. He Q, Yuan T, Yan X, Ding D, Wang Q, Luo Z, Shen TD, Wei S, Cao D, Guo Z (2014) Flame-retardant polypropylene/multiwall carbon nanotube nanocomposites: effects of surface functionalization and surfactant molecular weight. Macromol Chem Phys 215(4):327–340

9. Zhu J, Wei S, Li Y, Sun L, Haldolaarachchige N, Young DP, Southworth C, Khasanov A, Luo Z, Guo Z (2011) Surfactant-free synthesized magnetic polypropylene nanocomposites: rheological, electrical, magnetic, and thermal properties. Macromolecules 44:4382–4391

10. Purohit PJ, Huacuja-Sánchez JE, Wang DY, Emmerling F, Thünemann A, Heinrich G, Schönhals A (2011) Structure–property relationships of nanocomposites based on polypropylene and layered double hydroxides. Macromolecules 44(11):4342–4354

11. (a) Yang BX, Pramoda KP, Xu GQ, Goh SH (2007) Mechanical reinforcement of polyethylene using polyethylene-grafted multiwalled carbon nanotubes. Adv Funct Mater 17(13):2062–2069; (b) Xu D, Wang Z (2008) Role of multi-wall carbon nanotube network in composites to crystallization of isotactic polypropylene matrix. Polymer 49(1):330–338

12. (a) Fornes T, Paul D (2003) Crystallization behavior of nylon 6 nanocomposites. Polymer 44(14):3945–3961; (b) Homminga D, Goderis B, Dolbnya I, Reynaers H, Groeninckx G (2005) Crystallization behavior of polymer/montmorillonite nanocomposites. Part I. Intercalated poly (ethylene oxide)/montmorillonite nanocomposites. Polymer 46(25):11359–11365

13. (a) Trujillo M, Arnal M, Müller A, Laredo E, St. Bredeau, Bonduel D, Dubois P (2007) Thermal and morphological characterization of nanocomposites prepared by in-situ polymerization of high-density polyethylene on carbon nanotubes. Macromolecules 40(17):6268–6276; (b) Koval'chuk AA, Shchegolikhin AN, Shevchenko VG, Nedorezova PM, Klyamkina AN, Aladyshev AM (2008) Synthesis and properties of polypropylene/multiwall carbon nanotube composites. Macromolecules 41(9):3149–3156

14. Lei C, Chen D, Wu Y, Xu Y, Li S, Huang W (2011) Melt-grafting mechanism study of maleic anhydride onto polypropylene with 1-decene as the second monomer. J Appl Polym Sci 121(6):3724–3732

15. Babrauskas V, Peacock RD (1992) Heat release rate: the single most important variable in fire hazard. Fire Saf J 18(3):255–272

16. Wang X, Song L, Yang H, Xing W, Lu H, Hu Y (2012) Cobalt oxide/graphene composite for highly efficient CO oxidation and its application in reducing the fire hazards of aliphatic polyesters. J Mater Chem 22(8):3426–3431

17. (a) Yang H, Yang CQ, He Q (2009) The bonding of a hydroxy-functional organophosphorus oligomer to nylon fabric using the formaldehyde derivatives of urea and melamine as the bonding agents. Polym Degrad Stab 94(6):1023–1031; (b) He Q, Lu H, Song L, Hu Y, Chen L (2009). Flammability and thermal properties of a novel intumescent flame retardant polypropylene. J Fire Sci 27(4):303–321; (c) Nie S, Hu Y, Song L, He Q, Yang D, Chen H (2008) Synergistic effect between a char forming agent (CFA) and microencapsulated ammonium polyphosphate on the thermal and flame retardant properties of polypropylene. Polym Adv Technol 19(8):1077–1083

18. (a) He Q, Song L, Hu Y, Zhou S (2009) Synergistic effects of polyhedral oligomeric silsesquioxane (POSS) and oligomeric bisphenyl A bis(diphenyl phosphate)(BDP) on thermal and flame retardant properties of polycarbonate. J Mater Sci 44(5):1308–1316; (b) Zhang W, Li X, Guo X, Yang R (2010) Mechanical and thermal properties and flame retardancy of phosphorus-containing polyhedral oligomeric silsesquioxane (DOPO-POSS)/polycarbonate composites. Polym Degrad Stab 95(12):2541–2546

19. Beyler C, Hirschler M (1995) Thermal decomposition of polymers, chapter 7. In: SFPE handbook of fire protection engineering. National Fire Protection Association, and Society of Fire Protection Engineers, Boston, Massachusetts, pp 110–131

20. Singh B, Sharma N (2008) Mechanistic implications of plastic degradation. Polym Degrad Stab 93(3):561–584